Accounting for spectral shape in simplified fragility analysis of case-study reinforced concrete buildings

Stylianos Minas, and Carmine Galasso*

Department of Civil, Environmental & Geomatic Engineering and Institute for Risk & Disaster Reduction, University College London, London, UK

ABSTRACT

This paper deals with the selection of optimal intensity measures (IMs) for displacement-based seismic demand assessment and fragility derivation of case-study mid-rise reinforced concrete (RC) frames. The considered frames represent distinct RC vulnerability classes in the Mediterranean region. Optimal IM selection is performed by means of probabilistic seismic demand models considering multiple IMs and various engineering demand parameters (EDPs). Based on findings from previous and concurrent studies, a small subset of potential IMs is investigated here, including conventional peak IMs and two advanced scalar IMs accounting for spectral shape over a range of periods. Probabilistic seismic demand models are built on data obtained from analysis of the case-study frames subjected to over nine hundred ground motions by employing an innovative capacity spectrum method using inelastic response spectra derived from actual earthquake accelerograms to estimate seismic demand and derive fragility curves. This approach has the advantage of simplicity and rapidity over other methods as nonlinear dynamic analysis.

This study concludes that advanced IMs, and particularly the ones accounting for the period elongation (due to the nonlinear structural behavior) and structure-specific parameters, can effectively satisfy all the selection criteria, including the hazard computability criterion.

Keywords: *Intensity measures, Spectral shape, FRACAS, Fragility analysis*

1. Introduction

Recent earthquakes worldwide (e.g., the 1999 Izmit earthquake in Turkey; the 2009 L'Aquila earthquake in Italy; the 2016 Central Italy seismic sequence; the 2016 Ecuador earthquake) have resulted in extensive concentration of damage and significant economic losses in low seismic performance reinforced concrete (RC) buildings, and particularly mid-rise structures for both residential and commercial occupancy. The limited availability and poor quality (e.g., in terms of data aggregation) of historical damage data associated with several seismic-prone areas (e.g., [1]), makes the derivation of analytical fragility functions [2] an essential component of probabilistic seismic risk assessment. In particular, nonlinear dynamic analysis (NLDA) represents the analytical tool providing the most accurate approximation of the actual inelastic structural response. NLDA combines site- and/or structure-specific record selection and highly detailed nonlinear computational models capturing both monotonic and hysteretic structural behavior. However, such a level of detail is not always feasible or necessary, for instance, in catastrophe risk modelling applications [3] (e.g. large-scale earthquake risk assessment exercises). These applications focus on 'average' structural models for vulnerability assessment, often coupled with very limited exposure information, which are not compatible with the level of detail and computing required by NLDA.

In contrast, less complex, nonlinear static analysis procedures, which are often variants of the capacity-spectrum assessment methods, also exist. These procedures, such as the N2 method [4], FRACAS (FRAgility through CApacity Spectrum assessment) [5] among others, are widely implemented for fragility analysis of building classes, and rely on simplifying assumptions in assessing both the structural capacity and the seismic demand.

*Corresponding author.
E-mail address: c.galasso@ucl.ac.uk (C. Galasso).

Specifically, FRACAS, developed by the authors, uses suites of scaled and/or unscaled ground motion records (simply ground motions hereinafter) and quickly outputs a set of fragility functions for a considered index building[†]. One common, well-acknowledged, limitation of nonlinear static procedures is their inability of capturing ground motion spectral shape (e.g., [6]), which has been shown to have a significant influence on the estimated seismic response and resulting structural fragility. However, this limitation does not apply to FRACAS as it utilizes spectra from actual (real or simulated) ground motions to perform the structural assessment. The ability of FRACAS to properly account for ground motion spectral shape and its variability is further investigated in this paper. To this aim, the effect of implementing different combinations of intensity measure (IMs) and engineering demand parameters (EDPs) in simplified fragility analysis by FRACAS is explored herein.

In particular, one faces the question of how suitable the adopted IM is for representing ground motion uncertainty. This in turn will affect the required number of analysis and the accuracy of the resulting seismic demand estimates. Indeed, the development of fragility functions requires the choice of an IM which is 1) able to predict seismic demands involved in the considered performance objectives with the smallest scatter; and 2) providing a significant amount of information with respect to other ground motion features [7]. There are several recent papers explicitly addressing the selection of optimal ground-motion IMs intended to be used in performance-based assessment of existing structures, e.g., Mollaioli *et al*. [8] for RC base-isolated buildings, Bojórquez and Iervolino [9] for steel structures, Lucchini *et al*. [10] for torsional RC building subjected to bi-directional earthquake ground motion, Padgett *et al*. [11] for highway bridges portfolios, Kazantzi and Vamvatsikos [12] for analytical vulnerability loss assessment, Kohrangi *et al.* [13,14] for structural response estimation of RC buildings, Kohrangi *et al.* [15] for seismic loss assessment of 3D RC buildings, etc. A comprehensive overview of this previous research is not within the scope of this paper. However, it is worth noting that none of those past studies has focused on simplified demand assessment (and fragility analysis) based on nonlinear static (pushover-based) procedures for the seismic performance assessment of structures. In addition, only in recent years, advanced IMs (i.e., spectral-shape based) and innovative selection criteria (e.g., the relative sufficiency measure based on the information theory [7]) have been introduced and tested in separate studies (and for different structural types). The present study convolves all these state-of-the-art concepts and aims to identify optimal IMs to be used in probabilistic seismic demand analysis through nonlinear static procedures. Specifically, this paper aims to shed light in comparing different IM/EDP combinations for the fragility analysis of typical mid-rise RC frames by using FRACAS. For each case-study structure, different IMs are tested in order to identify an optimal IM or subset of optimal IMs, which can estimate structural response with minimum record-to-record variability, largest amount of information on ground motion features, yet hazard computable. Based on recent research findings, only a small subset of potential (and typical) IMs are considered in this study, namely peak ground acceleration (PGA), peak ground velocity (PGV), peak ground displacement (PGD), spectral (pseudo-) acceleration at the initial fundamental period (for a damping ratio of 5%), and two recently-proposed advanced scalar parameters accounting for spectral-shape over a range of periods. It is noted that integral (i.e., duration-based) IMs are omitted from this work as the effect of ground motion duration cannot be properly captured within the response spectrum inputs used in FRACAS. Moreover, it is widely known that duration has a secondary effect on displacement-based seismic demands, especially in the case of low-to-moderate ground motion intensities. Different local and global displacement-based EDPs are considered in the analysis. Three regular mid-rise (4-story) RC bare frames are selected as case-study structural models for this study. These structures provide representative examples of both the existing and the modern code-conforming European RC building stocks. Finite element models of these structures are developed in SeismoStruct [16] and analyzed using two sets of conventional static pushover analysis depending on the distribution of loads, namely uniform and triangular

[†] A real or fictitious building that represents the overall population by capturing its most important capacity and response characteristics [2].

pushover (PO) analysis. The resultant pushover curves are then transformed to capacity curves and implemented as inputs to FRACAS. Over 900 real (i.e., recorded during past events) ground motions are selected from the recent-developed SIMBAD database (*Selected Input Motions for displacement-Based Assessment and Design*; [17]). These records are used to estimate the seismic demand of each case-study building utilizing different EDPs.

In *Section 2*, the FRACAS approach is briefly reviewed, while *Section 3* introduced the considered IMs. *Sections 4* and *5* describe the case study buildings and the selection process for the ground motions used in the analysis. *Section 6* discusses the methodology steps followed in this study and *Section 7* outlines the most commonly used IM selection criteria, with particular focus on the ones utilized herein. Results and discussion are presented in *Section 8*, followed by *Section 9*, which compares the fragility functions obtained from two different IMs. Finally, *Section 10* presents some concluding remarks.

2. FRACAS - FRAgility from CApacity Spectrum assessment

In the current study, the simplified capacity assessment methodology, known as FRACAS is implemented in order to determine the performance points (PPs) of case-study structures for different ground motion inputs. FRACAS uses the basic methodology proposed in [9] and, through a new software tool built upon it, includes new features, such as more sophisticated capacity curve idealizations, the use of various hysteretic models for the single degree of freedom (SDoF) in the inelastic demand calculation, and the construction of fragility functions through several statistical model fitting techniques. The ability of FRACAS to consider multiple ground motions and building frames, makes it a powerful and efficient tool to account for the different sources of variability and evaluate the resulting uncertainties in the fragility prediction.

The step-by-step implementation of FRACAS procedure is described below (Figure 1):

1. A representative building, the so-called “index building”, is selected; variations of the index building, with differing structural detailing or geometrical characteristics, can also be generated. Computational models for each index building variation are developed.
2. Static pushover (PO) analysis or static adaptive PO (APO, e.g., [18]) is carried out to analyze the obtained computational models for each index building variation.
3. The resultant PO curve is transformed into a capacity curve in Acceleration-Displacement Response Spectrum (ADRS) space, taking into consideration the relative floor displacements and floor masses.
4. An idealized model is implemented to fit to the obtained capacity curve. There are several modelling options for this step, including the selection of the yielding and ultimate points, the number of fitting segments (bilinear or trilinear), and the presence of hardening/softening (e.g., Figure 1a).
5. The idealized curve is discretized into a number of analysis points (APs) (Figure 1b), where each AP represents an inelastic SDoF with the elastic stiffness, ductility and post-elastic properties shown by the capacity curve up to the considered AP. The number of APs can be selected by the user.
6. The response of the corresponding SDoF under the selected ground motion record is assessed at each AP through the Newmark-beta time-integration method. The elastic response is then computed for the APs preceding yield and the inelastic response for those on the inelastic branch(es) of the capacity spectrum (e.g. Figures 1c and 1d).
7. Both elastic and inelastic parts of the response spectrum are utilized to determine the PP as the intersection of the capacity curve and response curve. No iterative process is required.
8. The value of the selected EDP is back calculated from the capacity curve coordinates at the PP. Specifically, the PP coordinates are used to determine the corresponding load step of the nonlinear static analysis, and relevant response parameters are read from the analysis outputs. By default, FRACAS adopts maximum inter-story drift ratio (MIDR) as EDP, but others can be determined if required (e.g., roof drift, or RD). Different IMs associated with the given accelerogram used in the assessment are also calculated and stored.

9. The previous steps are repeated for different earthquake ground motions by either linearly scaling up a given record set (i.e., using a similar approach to the incremental dynamic analysis procedure [19]) to cover the desired range of intensities; or by using a larger record set selected to represent a wide range intensities of ground shaking (similarly to the cloud procedure; e.g., [20]). The number of PPs generated equals the product of the number of structural models, number of accelerograms and number of scaling factors used.
10. Based on the resultant set of IM and EDP pairs, fragility curves are generated through an appropriate statistical curve fitting approach.

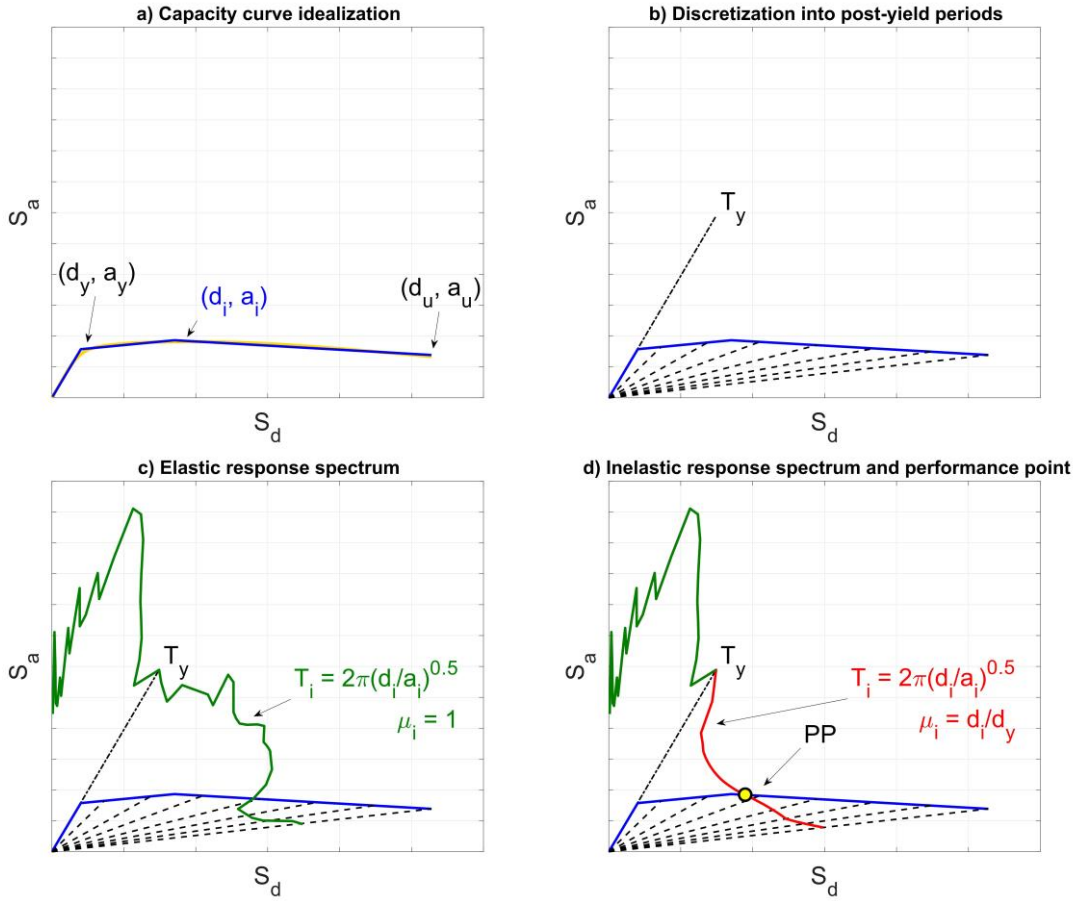

Figure 1. Main steps of FRACAS for the derivation of the performance point (PP) using the trilinear idealization model: (a) shows the fitting of the idealized trilinear curve to the structure capacity curve; (b) shows the identification of Analysis Points (AP), (c) compares the elastic demand spectrum with the capacity curve at the point of intersection of the demand curve with the line representing the yield period of the structure; (d) shows the determination of the PP.

For more details about the FRACAS procedure one may refer to [5]. It is noteworthy to mention that, in contrast to other capacity spectrum methods, FRACAS does not rely on reduction factors or indices to compute the inelastic spectrum from the elastic one. Instead, it carries out, for each target ductility and period, a simplified dynamic analysis on the idealized nonlinear SDoF model corresponding to the capacity curve. This process proves to be more time-consuming than the commonly-used static approaches, but it is more robust and remains faster than performing full time history analyses on finite element models of full structures.

This feature has also the advantage of permitting the use of various ground motions generating unsmoothed spectra as opposed to standardized design spectra. Therefore, the record-to-record variability can be directly introduced and the resulting cloud of PPs leads to fragility curves that account for the natural variability in the seismic demand.

3. Considered intensity measures

To identify the ground motion features most influencing the nonlinear response of a given structure of interest, several types of IMs can be considered. Conventional IMs (Table 1), including the peak ground responses (PGA, PGV and PGD) and spectral acceleration at the first period, $S_a(T_1)$, for 5% damping, are the most commonly used IMs. In general, PGA and $S_a(T_1)$ poorly predict the structural response of mid- to high-rise moment resisting frames (MRFs), although the latter IM can sufficiently capture the elastic behavior of first-mode dominated multi degree of freedom (MDoF) systems, especially in the case of low-to-moderate fundamental periods [21]. However, the behavior of highly nonlinear structures or structures dominated by higher-mode periods (less than T_1 - e.g., high-rise buildings) is not very well captured by utilizing $S_a(T_1)$ due to the lack of information on the spectral-shape provided by this IM. Therefore, it is essential to implement advanced IMs (Table 2) accounting for higher-mode/elongated periods, and/or considering nonlinear demand-dependent structural parameters (e.g. [22]). Kazantzi and Vamvatsikos [12] and Kohrangi *et al*. [13] amongst others have investigated the adequacy of numerous advanced scalar IMs taking into consideration the aforementioned parameters.

The first advanced scalar IM considered here is S_a^c (proposed by Cordova *et al*. [23]), which utilizes spectral-shape information (in terms of period elongation), and is expressed as:

$$S_a^c = S_a(T_1)\left[\frac{S_a(cT_1)}{S_a(T_1)}\right]^{\alpha} \tag{1}$$

where c and α are coefficients assumed to be $c = 2$ and $\alpha = 0.5$ respectively, based on the calibration carried out by the authors in the original study.

Bojórquez and Iervolino [9] also proposed the advanced scalar IM, I_{N_p}, which is based on $S_a(T_1)$ and the parameter N_p, defined as:

$$I_{N_p} = S_a(T_1)N_p^{\alpha} \tag{2}$$

where α parameter is assumed to be $\alpha = 0.4$ based on the tests conducted by the authors and N_p is defined as:

$$N_p = \frac{S_{a,avg}(T_1,...,T_N)}{S_a(T_1)} = \frac{\left[\prod_i^N S_a(T_i)\right]^{1/N}}{S_a(T_1)} \tag{3}$$

T_N corresponds to the maximum period of interest and lays within a range of 2 and $2.5T_1$, as suggested by the authors. In this study T_1 is assumed to be equal to 1s for all the considered buildings, as this is the representative natural period for mid-rise building class in catastrophe modelling; T_N is assumed to be equal to $2T_1$ (i.e. 2s); and only one intermediate period is considered (i.e., 1.5s). Ten different values, from 0.1 to 1, for the α-parameter are considered here in order to identify the optimal value for α, as discussed in the following sections.

Table 1. Conventional scalar IMs used in this study.

Intensity Measure	Name	Reference Study
$PGA = \max\left(\lvert a(t)\rvert\right)$	Peak ground acceleration	-
$PGV = \max\left(\lvert v(t)\rvert\right)$	Peak ground velocity	-
$PGD = \max\left(\lvert d(t)\rvert\right)$	Peak ground displacement	-
$S_a(T_1)$	Spectral acceleration at T_1	-

Table 2. Advanced scalar IMs used in this study.

Intensity Measure	Name	Reference Study
$S_a^c = S_a(T_1)\left[\frac{S_a(cT_1)}{S_a(T_1)}\right]^{\alpha}$	-	Cordova *et al.* (2000)
$I_{N_p} = S_a(T_1)N_p^{\alpha}$	-	Bojórquez and Iervolino (2011)

4. Case-study structures

Three regular RC 4-story, 4-bay bare frames, representing different vulnerability classes based on the building codes used for their design, are selected to illustrate the optimal IM selection. The selected case-study frames share the same geometry (bay widths and story heights) but are characterized by different material properties, cross-section dimensions, and reinforcement detailing. The first frame is designed to only sustain gravity loads following the Royal Decree n. 2239 of 1939 that regulated the design of RC buildings in Italy up to 1971, hereafter Pre-Code building [24]; the second frame is designed according the Decreto Ministeriale of 1972, hereafter Low-Code building [25]; and the third frame is designed according to the Italian seismic code of 2008 (or IBC08, fully consistent with Eurocode 8), following the High Ductility Class (DCH) rules, hereafter Special-Code building [26]. Inter-story heights, span of each bay and cross-sections dimensions for each case-study building are reported in Figure 2. The considered frames are regular (both in plan and in elevation). For more information about the design of those buildings, one may refer to De Luca *et al.* [27].

The finite element software SeismoStruct [16] is used to analyze the three case-study frames. The Mander *et al.* [28] concrete model is implemented, accounting for the effect of confinement. It is noted that an insufficient level of confinement is observed in all the cross-sections of the Pre-Code frame: the confinement factor, *k*, is defined as the confined-unconfined concrete compressive stress ratio and ranges from 1.01 to 1.05 for this case. The confinement factor for the case of Low-Code and Special-Code building reaches values up to 1.08 and 1.20 respectively. The Menegotto and Pinto [29] model is used to represent the hysteretic stress-strain behavior of reinforcing steel, calibrated with the parameters proposed by Filippou *et al*. [30] for the inclusion of isotropic strain-hardening effects. A distributed plasticity approach is used to account for material inelasticity, and each RC section is divided into a total of 150 steel, confined concrete, and unconfined concrete fibers.

Two sets of static PO analyses are carried out with different applied lateral load distributions, namely uniform and triangular. Lateral loads are incrementally applied to the side nodes of the structure. These lateral loads are proportionally distributed with respect to the local masses at each floor level (uniform distribution) and the inter-story heights (triangular distribution). In particular, uniform PO analysis is used for the cases of Pre- and Low-Code frames, as a local mechanism is considered to be more representative for buildings of these vulnerability classes; indeed, a soft-story failure mechanism at the ground level is observed due to shear failure of ground level columns. Triangular PO is deemed appropriate for the case of Special-Code building as a global failure mechanism is observed for this building type. In both cases, the PO analysis is carried out until a predefined target displacement is reached, corresponding to the expected collapse state. Although APO approaches are generally perceived to provide better estimates of structural response than conventional static PO, particularly when higher modes and structural softening are important (as shown in many previous

studies, such as [31]), it is decided not to adopt APO in the current comparison study. Inclusion of APO in FRACAS is computationally very expensive when dealing with a large number of unscaled accelerograms (as in the current study), as an APO needs to be developed for each accelerogram used.

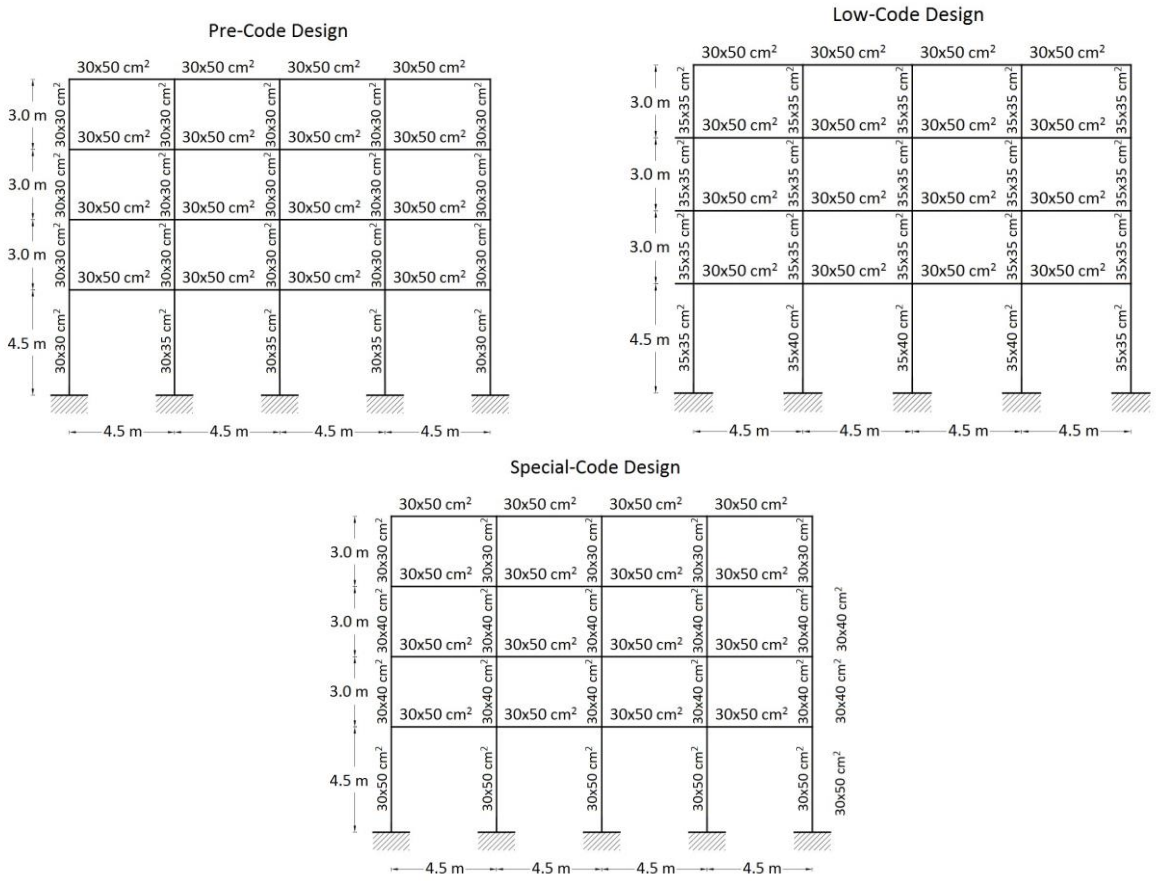

Figure 2. Elevation dimensions and member cross-sections of the considered RC frames.

Table 3 summarizes the structural and dynamic properties associated with each of the case-study building models, namely the mass of the system *m*, the actual fundamental period T_1 (based on Seismostruct estimations), and the assumed periods T_1* and T_N* used in the definition of the advanced IMs (as discussed in *Section 3*).

Table 3. Structural and dynamic information of each case study as required for the computation of different IMs.

Building	PO Analysis	Total mass [t]	T_1 [s]	T_1* [s]	T_N* [s]
Pre-Code	UNI	172.9	0.902	1.000	2.000
Low-Code	UNI	177.6	0.673	1.000	2.000
Special-Code	TRI	178.3	0.506	1.000	2.000

Figure 3a presents the static PO curves for the three-tested case-study buildings. The curves are reported in terms of top center of mass displacement divided by the total height of the structure (i.e., the roof drift ratio, RDR) along the horizontal axis of the diagram, and base shear divided by the building seismic weight along the vertical axis. This figure shows the capability of the structural model to directly simulate structural response up to collapse. Figure 3b shows the performance points in the ADRS space computed by FRACAS using the GMs records described in *Section 5* and the distributions of lateral loads associated to each case-study building.

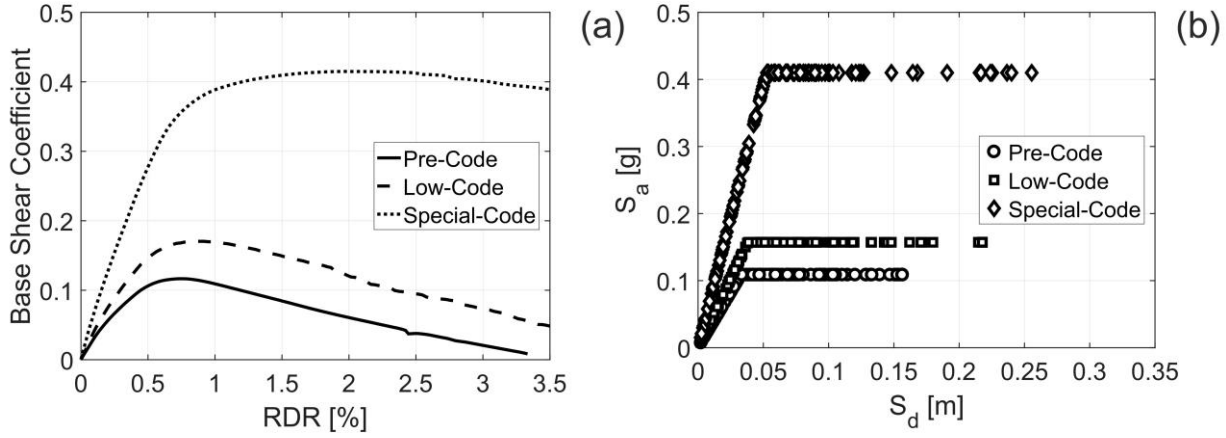

Figure 3. Static PO curves for the case-study buildings (a); and performance points generated by FRACAS using Elastic Perfectly Plastic (EPP) idealization model in the spectral acceleration-displacement space (b).

It is worth noting that different, more advanced capacity curve idealizations have been tested and critically discussed in [5] for the same case-study buildings. Findings from the study highlight that the choice of the idealization curve has a low impact on the obtained PPs and fragility curves, particularly when advanced statistical fragility fitting techniques are used. Consequently, a similar low impact of such a choice is expected on the optimal IM selection presented in this paper.

5. Ground motion database

The SIMBAD database (*Selected Input Motions for displacement-Based Assessment and Design*; [17]), used here, was developed in the framework of Rete dei Laboratori Universitari di Ingegneria Sismica (ReLUIS) 2010-2013 Project, as a strong ground motion database suitable for displacement-based design and assessment. A compendium of 467 records, consisting of two horizontal (X-Y) and one vertical (Z) components (1,401 recordings total), generated by 130 seismic events (including mainshocks and aftershocks) that occurred worldwide, form the aforementioned database. These accelerograms were assembled from various ground motion databases derived for different regions of the world following the selection criteria addressed below:

1. Shallow crustal earthquakes worldwide with moment magnitude (M) ranging from 5 to 7.3 and epicentral distance $R \leq 35$ km. This ensures to provide strong ground motion records of engineering relevance for most of the design conditions of interest that can be used without introducing large scaling factors.
2. Good quality at long periods, so that only records for which the high-pass cut-off frequency used by the data provider is below 0.15 Hz were considered. Therefore, most records are from digital instruments (about 80%), while from analogue instruments only those records with a good signal to noise ratios at long periods, typically from large magnitude earthquakes, were retained.
3. Availability of site class information based on quantitative criteria.

Figure 4 shows the distribution of magnitude and distance for the acceleration records compiled in the database. The records are grouped by site class according to Eurocode 8 [32] classification. Most of the records come from Japan (47%), Italy (18%) and USA (9%), New Zealand (16%) with minor contributions from European and Middle East countries, Turkey, Iran and Greece (10%).

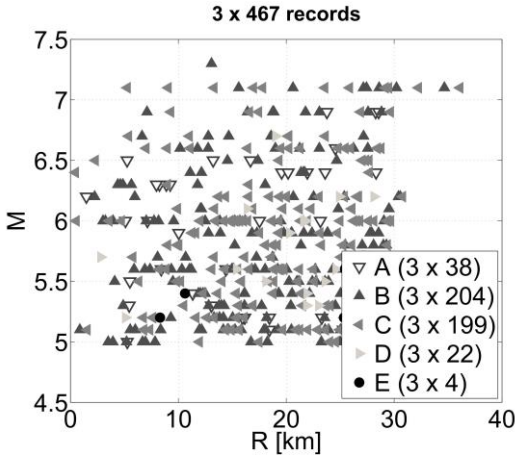

Figure 4. Moment magnitude versus epicentral distance distribution for SIMBAD dataset [17]**. The records are grouped by site class according to Eurocode 8** [32] **classification.**

6. Methodology

Statistical regression techniques are implemented here to determine the IM best predicting each considered EDP. To determine the statistical properties of the *cloud* response [33], the linear least squares is applied on EDP versus IM pairs for the suite of ground motions (unscaled) in order to estimate the conditional mean and standard deviation of EDP given IM. The simple power-law model in Eq. (7) is used here:

$$EDP = aIM^{b} \tag{7}$$

In Eq. (7), a and b are the parameters of the regression. The regression's standard deviation (s) is assumed to be constant with respect to IM over the range of IMs in the cloud and equal to:

$$s = \sqrt{\frac{\sum_{i=1}^{N}\left[\ln\left(edp_i\right) - \ln\left(a\ im_i^{b}\right)\right]^2}{N-2}} \tag{8}$$

In Eq. (8), edp_i and im_i are the EDP and IM values corresponding to the i-th ground motion - $\underline{edp_i}$ being calculated through FRACAS; N is the total number of ground motions. It is noteworthy to mention that significant heteroskedasticity may occur within some IM-EDP combinations and that this feature should be modelled explicitly when generating fragility functions [34]; for example performing linear regressions locally in a region of IM values of interest. Also, in the case of having vector IMs, a multivariate linear regression model can be easily applied. More advanced statistical approaches also exist, such as the Bayesian emulator-based approach recently proposed by one of the authors [35]. However, the use of a less complex approach is chosen here as it adequately serves the purposes of this study.

The power-law model illustrated in Eq. (7) can be simply re-written as shown below in Eq. (9), as a linear expression of the natural logarithm of the EDP and the natural logarithm of the IM:

$$\ln(EDP) = \ln(a) + b\ln(IM) + e \tag{9}$$

where e is a zero-mean random variable representing the variability of ln(EDP) given the IM. The use of logarithmic transformation indicates that the EDPs are assumed to be conditionally lognormally distributed (conditional upon the values of the IMs); this is a common assumption that has been confirmed as reasonable in many past studies. In the current study, the focus is laid on displacement-based EDPs, which are listed below:

1. peak (over time) inter-story drift ratio, as the largest difference between the lateral displacements of two adjacent floors, divided by the height of the story (denoted as *IDRi* for story *i*);
2. maximum (over all stories) peak inter-story drift ratio (denoted as *MIDR*);
3. ratio of the peak lateral roof displacement to the building height (i.e., *RDR*).

The abovementioned EDPs have demonstrated to be well correlated to both structural and non-structural damage, which contribute a major share of the total loss in an earthquake.

7. Optimal IM selection criteria

The choice of a given IM may have a significant effect on the uncertainty associated with the probabilistic seismic demand model and the resulting fragility curves. Therefore, the selection of optimal IMs is of high importance within the entire probabilistic seismic risk assessment process and consequently, raised the need for defining quantitative and qualitative selection criteria in order to facilitate these procedures. As discussed in the *Introduction*, several studies have been carried out to investigate aspects of ground motions that are responsible for the corresponding damage to particular elements or the system as a whole.

The most commonly used criteria for the determination of an optimal IM found in the literature include efficiency, sufficiency/relative sufficiency, practicality, proficiency, scaling robustness and hazard computability. However, in this study our main focus will be on the criteria listed below and reviewed in greater detail in the subsections *7.1-7.3*:

- Efficiency
- Sufficiency/Relative Sufficiency
- Hazard computability.

7.1 Efficiency

Efficiency is the most commonly used quantitative criterion for the determination of optimal IMs, and is related to variation of demand estimations for different values of a studied IM [11]. Specifically, more efficient IMs result in a reduced dispersion of the median EDP estimates conditional to a given IM. Thus, less analysis runs are required to narrow down the confidence intervals for those estimates.

The most efficient IM, that best predicts the EDP, is the one that provides the largest value of the coefficient of determination, R^2, among those considered or, equivalently, the one with the smallest value of standard deviation, *s*. R^2 is the proportion of variability in the EDP that is accounted for by the statistical model.

7.2 Sufficiency – Relative sufficiency

With regard to sufficiency, different approaches exist for the assessment of this metric. In particular, Padgett *et al*. [11], among others, define sufficiency as a criterion that characterizes the level of IM statistical independence conditional to specific earthquake characteristics, such as source-to-site distance (D) and magnitude (M). According to this approach, sufficiency is quantified based on the residuals dependence on M and D obtained through regression analysis [36]. Therefore, the estimations obtained from a sufficient IM are not correlated with the ground motion parameters M and D. However, the possible *p*-value analysis from such an approach provides only a binary evaluation of the IM (i.e., sufficient or insufficient) without offering any indication concerning the degree of insufficiency, when this is detected or, more in general, it doesn't explicitly quantify the relative performance of different, sufficient or insufficient, candidate IMs.

An alternative definition of sufficiency, known as *relative sufficiency*, was recently proposed by Jalayer *et al*. [7]. In particular, this measure investigates the relative sufficiency of a second IM, i.e. IM_2, with respect to a first one, IM_1. This measure is derived on the basis of information theory concepts and quantifies the suitability of one intensity measure relative to another. Specifically, the relative sufficiency measure, denoted herein as $I(EDP|IM_2|IM_1)$, is equal to the average difference

between the information gained (measured in terms of Shannon entropy or simply entropy [37]) about the performance variable EDP given IM_1 and IM_2 and that gained given IM_1 only. If $I(EDP|IM_2|IM_1)$ is positive, this means that on average IM_2 provides more information about EDP than IM_1; hence, IM_2 is more sufficient than IM_1. Similarly, if $I(EDP|IM_2|IM_1)$ is negative, IM_2 is less sufficient than IM_1. This is numerically expressed as:

$$I\left(EDP \mid IM_2 \mid IM_1\right) \cong \frac{1}{N}\sum_{i=1}^{N}\log_2 \frac{p\left[EDP = edp_i \mid IM_1\right]}{p\left[EDP = edp_i \mid IM_2\right]} \tag{10}$$

In Eq. (10), the probability density function (PDF) $p\left[EDP_i \mid IM\right]$, considering a lognormal distribution with the parameters defined through the cloud analysis, is calculated as follows:

$$p\left[EDP = edp \mid IM\right] = \frac{1}{edp \cdot s}\phi\left(\frac{\ln edp - \ln\left(a\ im^b\right)}{s}\right) \tag{11}$$

where $\phi(\bullet)$ is the standardized Gaussian PDF. Hence, the relative sufficiency measure can finally be expressed as:

$$I\left(EDP \mid IM_2 \mid IM_1\right) \cong \frac{1}{N}\sum_{i=1}^{N}\log_2 \frac{s_1}{s_2}\frac{\phi\left[\left(\ln edp_i - \ln\left(a_2\ im_2^{b_2}\right)\right)/s_2\right]}{\phi\left[\left(\ln edp_i - \ln\left(a_1\ im_1^{b_1}\right)\right)/s_1\right]} \tag{12}$$

In Eq. (12), $\left(a_1, b_1, s_1\right)$ are the cloud parameters corresponding to IM_1 while $\left(a_2, b_2, s_2\right)$ are the cloud parameters corresponding to IM_2, and N is the total number of ground motion records. More details on the derivation of Eq. (12) are provided in [7]. The relative sufficiency measure is estimated for each performed cloud analysis and is measured in units of bits of information. According to Jalayer et al. [7], the relative sufficiency measure provides a preliminary ranking of candidate IM_2 with respect to the reference IM_1. The approximation of Eq. (12) can be used for a fast screening of various candidate IMs; however, it can, in some cases, lead to inaccurate results [38]. To account for these inaccuracies, Jalayer et al. [7] proposed a refined method, based on a stochastic ground motion model combined with disaggregation of the seismic hazard at the site, and employing Monte Carlo simulation to estimate the expectation involved in the formal definition of the relative sufficiency measure. It is noteworthy mentioning that the estimates of the refined method generally show good agreement with the rough preliminary estimates, although in some cases the refined modelling results in slightly different rankings of the candidate IMs. However, the use of the approximation of Eq. (12), is still considered to be an adequate option for comparing different IMs without the need to use the refined approach [38].

7.3 Hazard computability

According to the definition given in [39], hazard computability describes the process to obtain the earthquake hazard at a given site in terms of a considered IM. Numerous hazard maps and Ground Motion Prediction Equations, GMPEs (or attenuation laws) exist for the most commonly used IMs, namely PGA and spectral ordinates at given periods (representing sometimes a restricted range of possible discrete periods), making these IMs more favorable from the hazard computability perspective; whereas, other IMs (spectral ordinates at the actual fundamental and/or elongated periods and advanced IMs) may require interpolation or supplementary structural or dynamic information, making the computation of the hazard a more time-consuming process.

8. Results and discussion

In this section all the considered IMs are assessed based on the selection criteria discussed in *Section 7*. Specifically, the overall performance of each considered IM, for each considered EDP (computed through FRACAS), is obtained based on the comparison of the quantitative parameters associated with each testing criterion. For sake of brevity, only two individual case studies, namely the Pre- and Special-Code buildings subjected to uniform and triangular PO loads respectively, are selected to show the optimal IM selection process discussed in this study, and therefore determine the optimal IM for the fragility analysis of each particular building class. However, the same process has also been applied to the Low-Code case-study building and the results of the analysis are essentially consistent with the observations obtained from the Pre-Code case study frames. It is also worth noting that, to incorporate modeling uncertainties in the assessment of seismic demand assessment of the case-study buildings, samples of the material, geometrical, and mechanical parameters for each structural model could be generated and analyzed subjected to the considered suite of earthquake ground motion records. However, the focus here is on investigating the use of record-to-record variability in nonlinear static capacity approaches for fragility assessment.

As shown in Figure 3(a), the two selected structures behave highly nonlinearly over a threshold of approximately 0.40% and 0.65% RDR for the Pre- and Special-Code buildings respectively. The ground motion records not "pushing" the considered structures into the nonlinear range are discarded from the IM-EDP datasets used herein. It is noted that FRACAS, as a capacity spectrum-based method, utilizes an equivalent SDoF system to represent the behavior of the modelled building and, by definition, $S_a(T_1)$ represents the response of a linear elastic SDoF. As a result, the seismic intensity and the estimated FRACAS response are perfectly correlated within the elastic regime. Based on this, the actual number of GM that pushed the frame into the nonlinear range is relatively small but still significant, corresponding to approximately 15% and 25% of the total number of records used, for the case of Special- and Pre-Code buildings respectively (i.e. 70 and 110 GMs, as shown in Figure 3(b)).

Figures 5 and 6 illustrate the scatter plots of the structural seismic demand in terms of MIDR versus the scalar candidate IMs for the considered ground motion subset and for each selected case-study structure. Note that for the calculation of I_{N_p} values presented in these figures, a single α-parameter is used for each case study building, based on the optimal calibration process described later in this section. These figures also show the median and two standard deviations above and below the median, respectively, from the logarithm regression model fitted to the data. With regard to efficiency, the visual inspection of Figures 5 and 6 confirms that displacement-based EDPs, such as MIDR, is better correlated with the spectral shape parameter I_{N_p} for all studied cases (lowest value of standard deviation, *s*). In contrast, the peak ground parameters, namely PGA and PGD, are confirmed to be poor predictors of the nonlinear structural response of mid-rise moment resisting frames (highest values of standard deviation), while PGV performs reasonably well in the case of the Special-Code building and poorly in the case of the Pre-Code case-study building. As expected, $S_a(T_1)$ appears to be the most efficient conventional IM in all cases, closely matching the performance of I_{N_p} for the Special-Code case study. Finally, S_a^c performs consistently well in terms of efficiency for all tested case studies.

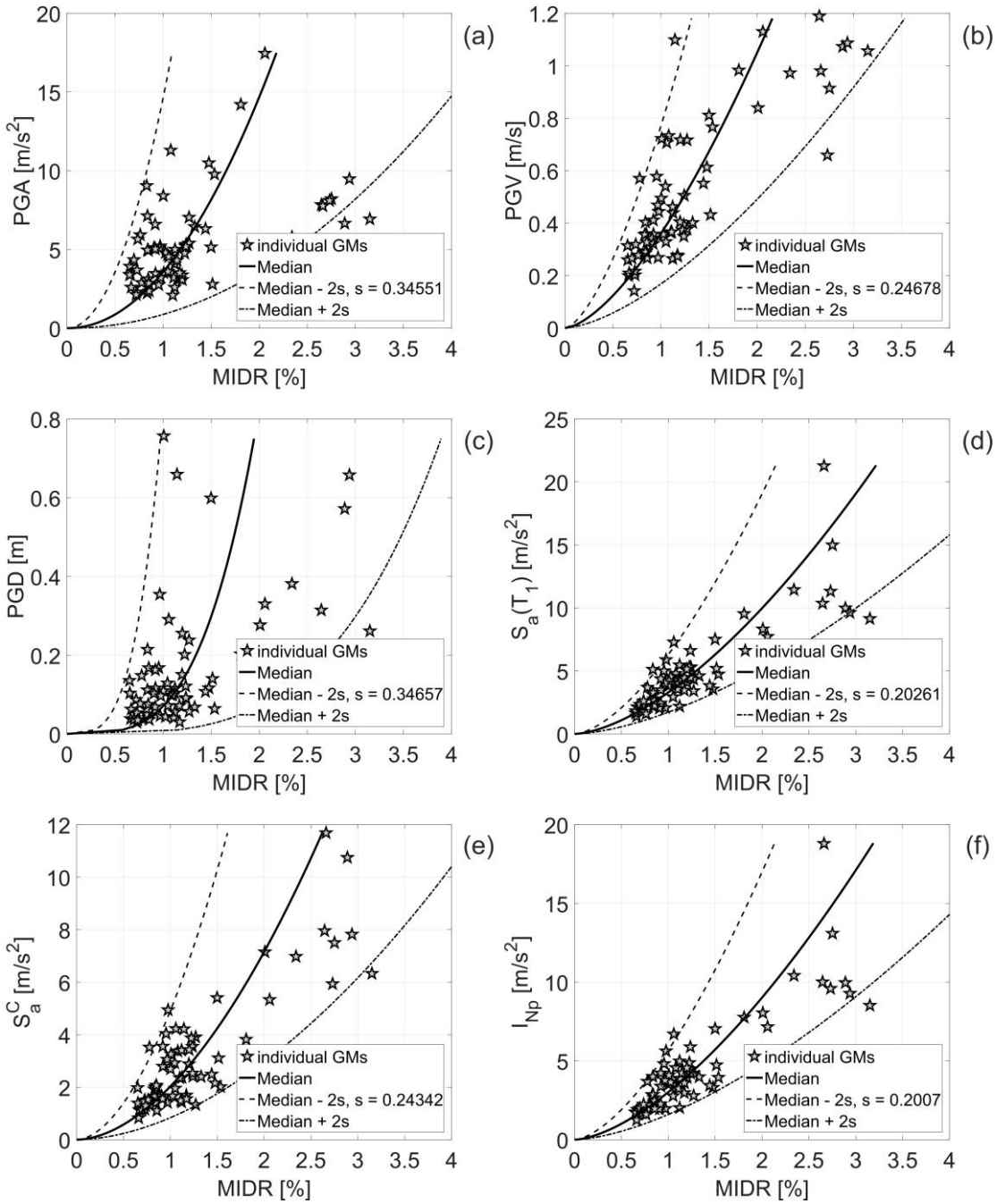

Figure 5. Scatter plots of the adopted IMs versus MIDR for the considered subset of ground motion records (Special-code building, Triangular PO).

As expected, the superiority of the advanced IMs becomes more evident for the case study buildings experiencing highly nonlinear demands, such as Pre- and Low-Code buildings, as these IMs can account for the effect of period elongation. On the other hand, the superiority of advanced IMs is less apparent for the Special-Code building, although it is nominally designed to provide higher nonlinear capacity/ductility than the Pre- and Low-Code buildings. This is due to the high strength level (e.g., in terms of base shear coefficient) characterizing the Special-Code case-study structure. In fact, only a small number of the selected ground motion set actually "pushes" the building into the nonlinear range (70 records), making more difficult to exploit the nonlinearity assumed in the design.

A potential improvement in the performance of the advanced IM, I_{N_p} may be achieved by calibrating the α-parameter in its definition for the specific case study structures rather than using the values suggested by other researchers for different case study structures. It is noted that a case-study specific

calibration of the α-parameter can be a time-consuming process which cannot always be practically implemented in a seismic performance assessment study. However, the calibration outcome presented here is consistent with other cases performed by the authors (RC buildings of different heights and vintages [40]) and to that of steel MRFs presented in the original study proposing I_{N_p} [9]. These similarities should provide confidence in using the range of α-values obtained here to the seismic performance assessment of buildings of similar characteristics [40]. In particular, ten different sets of α-values are tested, ranging from 0.1 to 1.0, and the associated I_{N_p} - MIDR relationship dispersions are computed and compared to dispersion of the other candidate IMs for all three buildings, as shown in Figure 7.

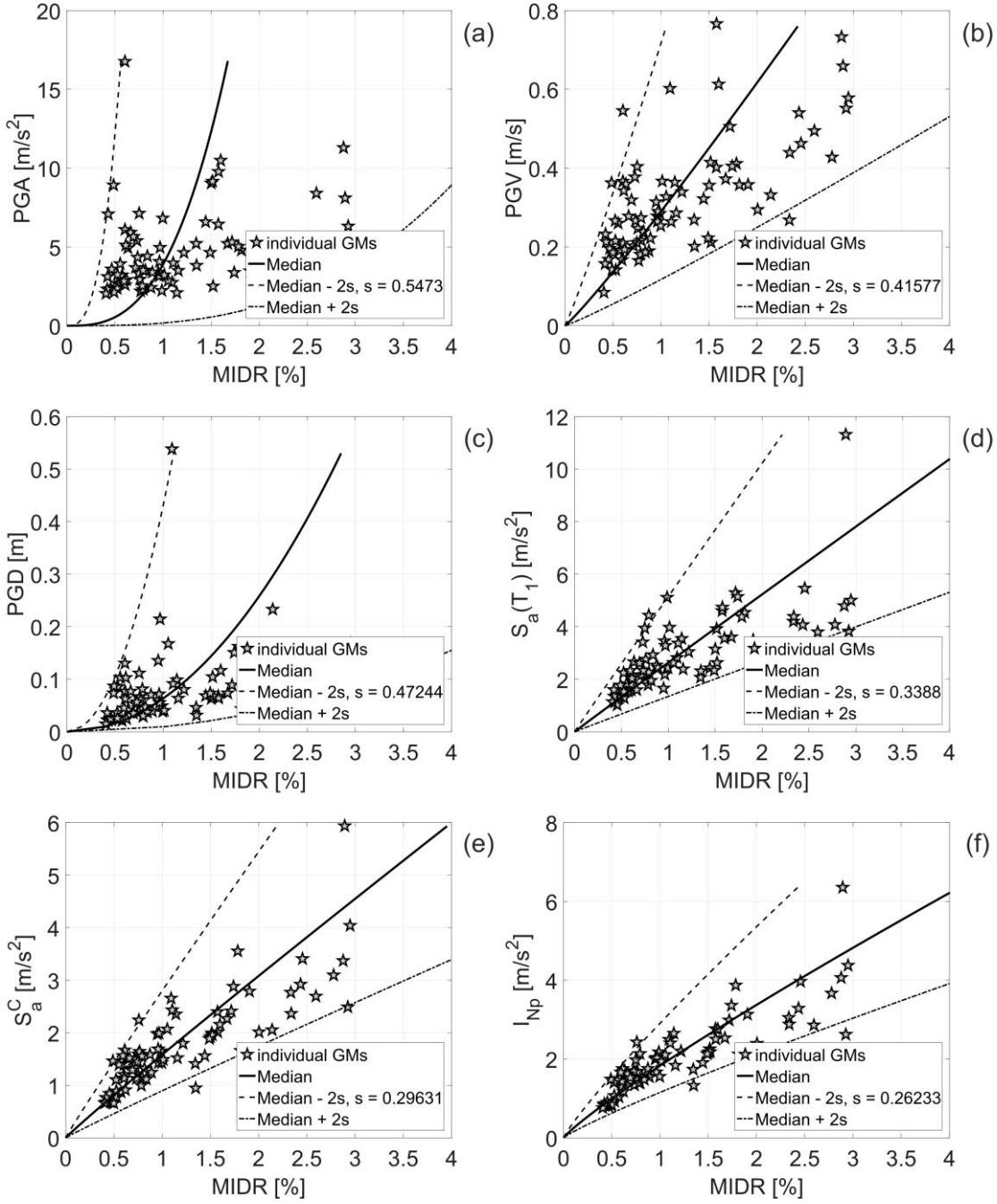

Figure 6. Scatter plots of the adopted IMs versus MIDR for the considered subset of ground motion records (Pre-code building, Uniform PO).

When the α-parameter approaches values close to zero, I_{N_p} approximates $S_a(T_1)$, which also becomes apparent when comparing the standard deviations of the EDP-$I_{N_p}(\alpha = 0.1)$ and EDP-$S_a(T_1)$ models (Figure 7), resulting in almost identical *s*-values. Similarly, when the α-parameter values tend to one, I_{N_p} approximates the average spectral acceleration, *AvgSA*, over three periods, namely 1, 1.5 and 2s. The latter case practically means that spectral accelerations corresponding to periods greater than T_1 (i.e. 1.5 and 2s – elongated periods) contribute equally in the estimation of MIDR. As discussed above, the Special-Code building is characterized by more nominal inelastic displacement capacity and ductility; however, the use of *cloud* analysis coupled with the specific, yet realistic, ground motion set selected herein do not allow one to exploit those. While this is a well-known limitation of the *cloud* analysis approach as opposite to incremental dynamic analysis (see results in [12]), the ground motion set used here consists of the strongest records in the SIMBAD database and the corresponding IM values are hazard-consistent, even at very higher return periods, as it will be shown in the next section. This explains why the optimal α-parameter for the case of Special-Code building is equal to 0.2. In contrast, the optimal α-parameter for Pre- and Low-Code buildings is equal to 0.7 and 0.8 respectively, as a bigger number records "push" the building to the nonlinear range of behaviors where period elongation occurs.

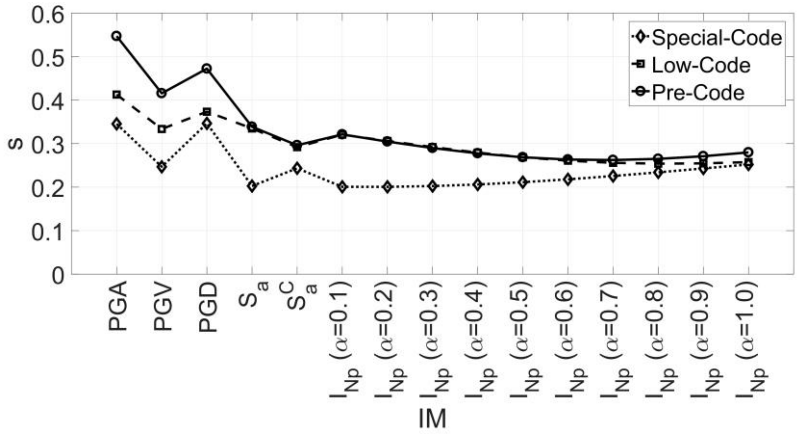

Figure 7. Standard deviation (dispersion) of residuals of MIRD for the considered IMs and each case-study building.

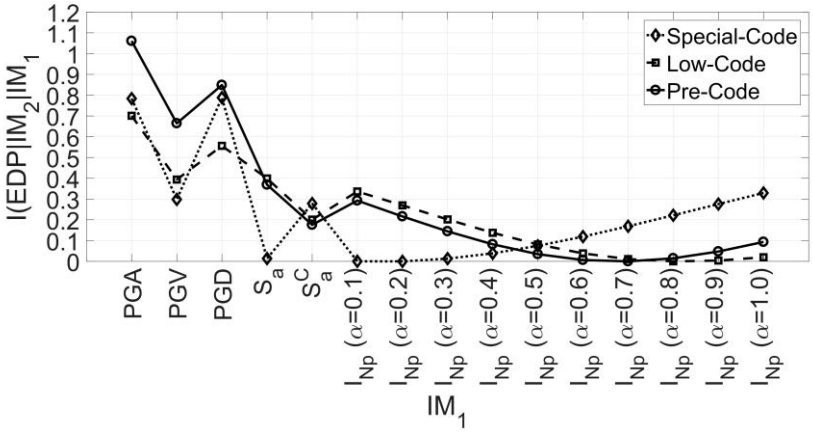

Figure 8. Relative sufficiency measure for alternative IMs with respect to the IM with the lowest dispersion (Figure 7) for each case-study building.

The relative sufficiency measure for MIDR and the candidate IMs is presented in Figure 8 for all three buildings. The reference IM_1 is chosen here as the one corresponding to the lowest *s* value from

the regression (Figure 7). The results in Figure 8 confirm the results in terms of efficiency (Figure 7). The IMs resulting in the highest efficiency are also characterized by the highest relative sufficiency. Next, the study investigates the sensitivity of the dispersion of residuals of MIDR for the considered IMs to the number of periods used to compute I_{N_p}. Ten equally spaced successive periods between 1 and 2s are utilized to recalculate I_{N_p}. Figure 9 shows the new dispersion estimates for the recalculated I_{N_p} (grey lines) and how they compare the previous dispersion estimates, where only three periods (i.e. 1, 1.5 and 2s) are used (black lines). The results in Figure 9 confirm the results shown in Figure 8, regarding the optimal α-parameter calibration. Additionally, this test reveals that the use of a bigger number of periods does affect the resultant performance of I_{N_p}, but not necessarily in a positive way.

The use of more periods results in a reduction of the dispersion of MIDR residuals for the cases of Pre-(-0.7 to -4.4%) and Low-Code buildings (-1.0 to -10.3%), while it has a counter effect in the case of Special-Code, as the associated dispersions tend to increase (+0.2 to +4.2%). This is again attributed to small number of records actually "pushing" the Special-Code building deep in the nonlinear regime. As a result, the effect of the additional spectral accelerations corresponding to higher periods not only is not adding any additional information but is also having an adverse impact in the resultant standard deviation estimates.

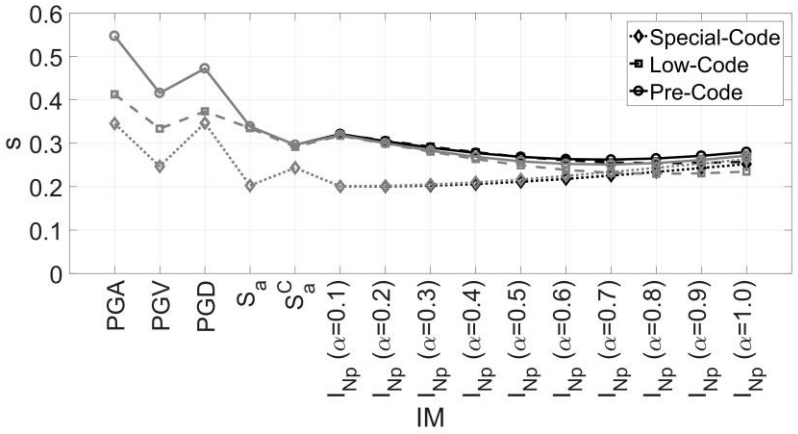

Figure 9. Sensitivity of the standard deviation (dispersion) of residuals of MIRD for the considered IMs and each case-study building to the number of periods used to compute I_{N_p} (grey lines correspond to 10 equally-spaced periods between 1s and 2s).

It is worth noting that, given the complex relationship between ground motions and nonlinear structural response and the difficulty of capturing relevant ground motion features with a single parameter, it is unlikely that a scalar IM will render nonlinear structural response conditionally independent of all other ground motion parameters. The same is true for a vector IM that uses only a small number of parameters. In the context of practical applications, as those presented in this study, a sufficient IM is the one minimizing the influence of the ground motion set that is used to estimate seismic demands. This also implies that the careful record selection and/or modification required to obtain a good estimate of the structural performance may not be required or may be significantly reduced if advanced IMs are used.

The last criterion for the determination of an optimal IM is the hazard computability. For this criterion, conventional IMs have a significant advantage over advanced IMs, as numerous GMPEs and hazard maps exist particularly for PGA, PGV and PGD, and some spectral ordinates for specific ranges of periods. On the other hand, it is still possible to derive GMPEs for some of the advanced IMs, namely I_{N_p} and S_a^c, using either *direct* or *indirect* methods. In particular, Kohrangi et al. [41], derived empirical GMPEs for the average spectral acceleration, *AvgSA*, defined as the geometric mean of

spectral acceleration values over a range of periods (i.e., for I_{N_p} with $\alpha = 1$). As pointed out by the authors (and also in [9]), one of the advantages of the advanced, spectral-shape-based IMs, stands on the assumption that their distribution is computable from the available GMPEs for spectral acceleration, GMPE-*SA*, (indirect method) without the need for deriving new specific GMPEs for *AvgSA*, GMPE-*AvgSA*, (direct method). The results in [41] show that the indirect approach yields median *AvgSA* estimates that are identical to those of the direct approach. However, the estimates of *AvgSA* variance of the two methods are identical only if both the GMPE-*SA* and their empirical correlation coefficients among different *SA* ordinates are derived from the same record dataset.

8.1 Example of hazard computability in terms of I_{N_p}

An illustrative example of site-specific probabilistic seismic hazard analysis (PSHA) in terms of I_{N_p} with $\alpha = 0.7$ is presented here. Such a PSHA is carried out by using a Monte Carlo simulation-based approach (e.g.,[42]), accounting for uncertainty in all the factors affecting ground motions at a given site. Specifically, the town of Avellino in the Campania region of Southern Italy is used here as a case-study site. Avellino is characterized by high seismicity, with two major events occurred in the last 90 years (i.e., the M6.7 on 27/7/1930, and M6.9 on 23/11/1980). To perform PSHA for Avellino, a synthetically generated set of potential earthquakes, with their temporal and geographical distribution, is developed by drawing random samples from the assumed PSHA model components (and related probability distributions), i.e., source-zone geometries and magnitude-recurrence parameters and maximum magnitude. The official Italian seismogenetic zonation, named ZS9 ([43]), is used in this study; the calculation is limited to events with source-to-site distance up to 100 km (Figure 10). Gutenberg-Richter parameters implemented for generating each record are adapted from [44].

The resulting synthetic catalogue has a duration of 5,000 years; each record of the synthetic catalogue contains the following fields: time (in decimal years), coordinates (latitude and longitude) and magnitude of earthquake, source zone number and corresponding fault-style. In fact, ZS9 assigns a prevalent mechanism of faulting – interpreted as the mechanism with the highest probability of generating future earthquakes – to all its source zones for use in the GMPEs.

The considered IM is evaluated for each seismic event contained in the catalogue by using the indirect approach and models presented in [41], assuming type B ground. 500 realizations of random numbers drawn from the standard normal distribution is multiplied by the given sigma value (variability of the GMPE model) and added to the median log-ground motions (from the GMPE) to model the aleatory variability in ground motions. The resulting site-specific hazard curves for each realization (light grey color) as well as the median, 16th and 84th hazard curves (blue color) are shown in Figure 11.

The actual possibility of computing hazard analysis is crucial for the usefulness of the proposed optimal IMs. It is worth noting, as discussed in [12], that within a risk assessment framework, the reduction in response dispersion gained by a more efficient IM, does not reduce the overall risk variability. A different IM is simply ‘a different partitioning of the sample space for applying the total probability theorem on which the risk calculation is based upon’ (e.g., [12]). Thus, part of the variability is simply shifted to a different level within the risk assessment, and in particular to the seismic hazard curve definition. By definition a more efficient IM is more structure specific, therefore, higher dispersions are obtained when trying to define an appropriate GMPE. In other words, no matter the adopted IM, as long as sufficiency is maintained, the same overall variability at the end of the risk assessment, i.e. after convolving the vulnerability with the hazard, should be observed. However, shifting a part of the variability from the response analysis level towards the probabilistic hazard analysis level has a major advantage, a significant reduction in the computational costs associated to the structural analysis.

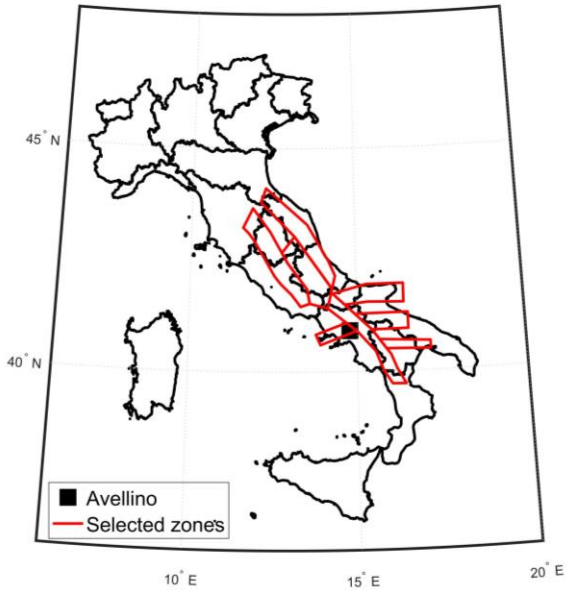

Figure 10. Case-study location (Avellino) and considered ZS9 seismic sources.

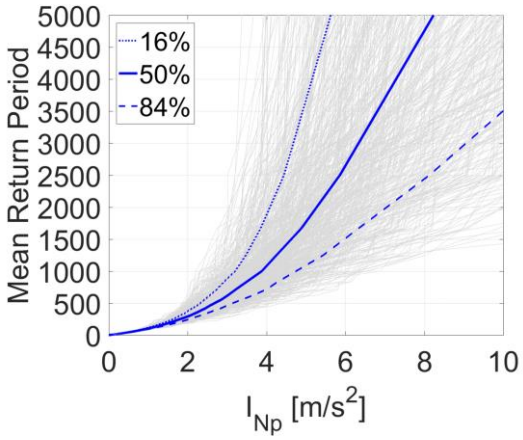

Figure 11. Site-specific hazard curves for Avellino in terms of I_{N_p} with α = 0.7.

9. Fragility assessment

In this section, two sets of fragility functions are presented, one for the conventional IM, $S_a(T_1)$, and one for the advanced IM, I_{N_p}, using the optimal α-parameter as calibrated for each vulnerability class. These IMs are chosen to represent the conventional and advanced IMs respectively, due to their overall performance in the tests conducted in *Section 8*. The fragility curves are derived from the FRACAS analysis results by adopting thresholds of MIDR to define three damage states. Table 4 shows the descriptions and the thresholds associated with each damage state, which are used for the derivation of the fragility curves. This damage scale is based on the re-interpretation of the Homogenized Reinforced Concrete (HRC) damage scale proposed by [45] and that in [46]. More details on the adjustments of this damage scale to the case-study buildings can be found in [5]. Figure 12 presents the locations of damage states along the static PO curves for the three case-study buildings.

As in *Section 8*, only two case-study buildings, namely the Pre- and Special-Code buildings, are used to demonstrate the derivation of fragility curves for the selected optimal IMs. Figures 13 and 14 illustrate the median fragility curve sets expressed in terms of $S_a(T_1)$ (left panel) and I_{N_p} (right panel), and their associated 95% confidence intervals estimated using the bootstrap technique for Pre- and Special-Code buildings respectively. In brief, a large number of bootstrap samples (1,000 in this case)

are simulated and a fragility function is drawn for each bootstrap iteration and consequently the 95% bootstrap confidence intervals are computed. For more details about the derivation of bootstrap confidence intervals one may refer to [47]. It is noted that only the first two damage states are shown in Figure 14, as the partial collapse damage state (DS3) is not reached for this case study for the particular suite of records used herein.

Visual inspection is considered to be an acceptable means of comparison of fragility curves due to the difficulty of addressing a numerical goodness of fit measure [48]. A steep fragility curve indicates a significant explanatory power of the IM in question, while the width of confidence intervals describes the level of dispersion.

Table 12 - Description of damage states and damage state thresholds used in this study.

HRC Damage State	DS1 Moderate	DS2 Extensive	DS3 Partial Collapse
Observed Damage	Cracking in most beams and columns. Some yielding in a limited number. Limited concrete spalling	Ultimate strength is reached in some elements	Failure of some columns or impending soft-story failure
Response Characteristics (Threshold defined by the first occurrence of any of these)	Global yield displacement, as obtained by the idealized curve.	Maximum moment capacity of a supporting column is reached.	- There is a drop in strength to 80% of the maximum global capacity; - Shear failure of one element; - The rotation capacity of a critical column is reached.
MIDR Threshold Pre-Code structure (%)	0.49	1.53	3.00
MIDR Threshold Low-Code structure (%)	076	1.89	4.27
MIDR Threshold Special-Code structure (%)	0.95	2.11	5.62

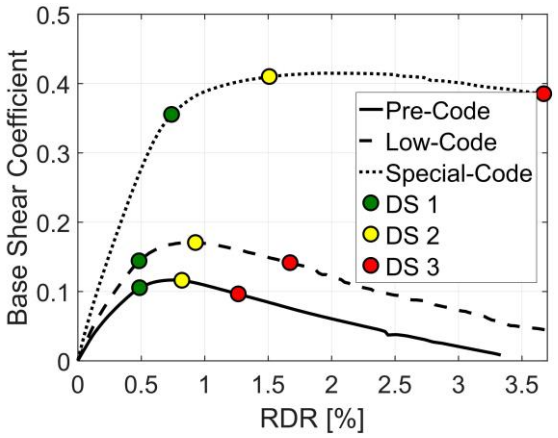

Figure 12. Static PO curves for the case-study buildings with associated damage thresholds.

As a result, the visual comparison of the two fragility curves sets shown in both Figures 13 and 14 reveal an apparent superiority of the I_{N_p} comparing to the $S_a(T_1)$) fragility curves. The use of the

advanced IM, I_{N_p}, results in steeper fragility curves for both damage states 1 and 2, and also narrower confidence intervals. This improvement is less obvious for the case of Special-Code building for the reasons extensively discussed in *Section 8*. In addition, $S_a(T_1)$ showed to perform considerably well, almost matching the performance of I_{N_p}, for cases where the impact of nonlinearity is limited or not fully exploited.

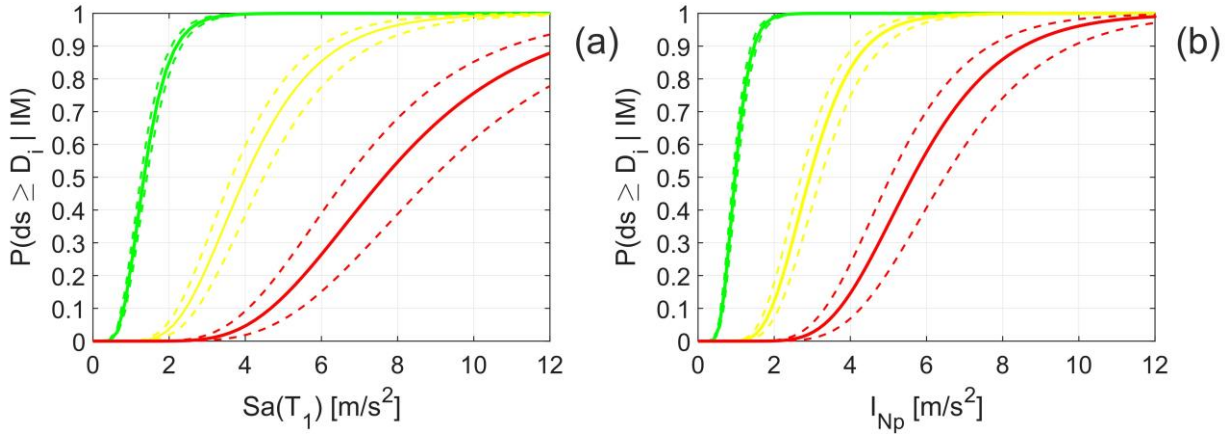

Figure 13. Fragility curves and their 95% confidence intervals derived for Pre-Code building, expressed in terms of *Sa(T₁)* (a) and *I_{Np}* (b).

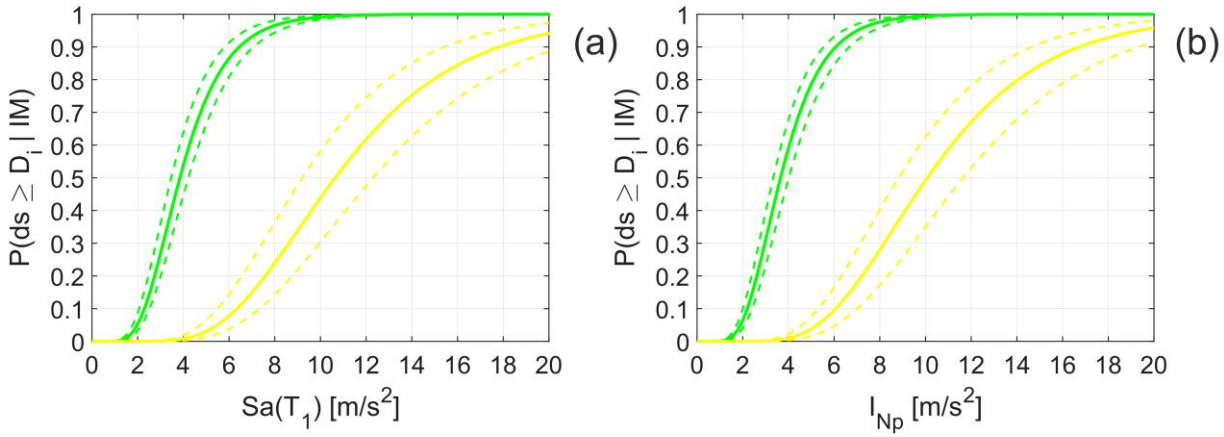

Figure 14. Fragility curves and their 95% confidence intervals derived for Special-Code building, expressed in terms of *Sa(T₁)* (a) and *I_{Np}* (b).

It is worth noting that the current study could be further extended towards a full seismic risk assessment for the case-study buildings given that the two ingredients needed (i.e., hazard and fragilities - computed for different damage states) are now readily available.

10. Conclusions

This paper presented an investigation aiming at identifying the ground motion IMs that are better correlated with displacement-based response parameters for simplified fragility analysis of mid-rise RC buildings. The selection of an efficient, sufficient, and hazard computable IM is an important task towards developing analytical vulnerability curves and consequently assessing the seismic losses for a building class. For this purpose, three case-study existing RC frame buildings, typical of the Italian-Mediterranean inventory of different vintages were considered. To establish correlations between IMs and EDPs describing the nonlinear performance of the case-study structures, a comprehensive set of ground motions and an innovative capacity spectrum method that uses inelastic response spectra derived from actual earthquake accelerograms were used. Six alternative ground motion IMs,

including advanced IMs accounting for spectral shape, have been considered. Efficiency, sufficiency and relative sufficiency, and hazard computability were recognized as the main criteria for judging the adequacy of each candidate IM in this study and selecting the optimal IM. The outcomes of the present work are consistent with previous investigations conducted by the authors and other researchers on selecting optimal IMs (scalar or vector-valued) for predicting structural response by using computationally demanding, full nonlinear dynamic analysis. In fact, it has been demonstrated that a successful IM might be formed by specifying an appropriate period range that includes periods above the mean first mode period (thus accounting for inelastic period elongation) and combines the associated spectral acceleration values via the geometric mean. In particular, an IM that uses only three such periods was found to perform best in terms of efficiency and relative sufficiency across the entire practical range of local (i.e., at story level) and global EDP for each case-study structure In general, this type of advanced IMs comfortably satisfy all the selection criteria, including the hazard computability criterion. Indeed, the study showed how probabilistic seismic hazard analysis for I_{N_p} can be easily performed with existing tools.

Acknowledgements
The first author would like to acknowledge the UK Engineering and Physical Sciences Research Council (EPSRC) and AIR Worldwide Ltd through the Urban Sustainability and Resilience (USAR) EngD programme at University College London (UCL) for funding for his research work. The authors are very grateful to Prof. Tiziana Rossetto for her contribution on an earlier version of this work.

References

[1] Ioannou I, Douglas J, Rossetto T. Assessing the impact of ground-motion variability and uncertainty on empirical fragility curves. Soil Dyn Earthq Eng 2015;69:83–92. doi:10.1016/j.soildyn.2014.10.024.
[2] D'Ayala D, Meslem A, Vamvatsikos D, Porter K, Rossetto T, Crowley H, et al. Guidelines for Analytical Vulnerability Assessment - Low/Mid-Rise. GEM Tech Rep 2013;08:162. doi:10.13117/GEM.VULN-MOD.TR2014.12.
[3] Mitchell-Wallace K, Jones M, Hillier J, Foote M. Natural Catastrophe Risk Management and Modelling: A Practitioner's Guide. Wiley-Blackwell; 2017.
[4] Fajfar P. Capacity spectrum method based on inelastic demand spectra. Earthq Eng Struct Dyn 1999;28:979–93. doi:10.1002/(SICI)1096-9845(199909)28:9<979::AID-EQE850>3.0.CO;2-1.
[5] Rossetto T, Gehl P, Minas S, Galasso C, Duffour P, Douglas J, et al. FRACAS: A capacity spectrum approach for seismic fragility assessment including record-to-record variability. Eng Struct 2016;125:337–48. doi:10.1016/j.engstruct.2016.06.043.
[6] Silva V, Akkar S, Baker JW, Bazzurro P, Castro JM, Crowley H, et al. Current Challenges and Future Trends in Analytical Vulnerability Modelling (under review). Earthq Spectra n.d.
[7] Jalayer F, Beck JL, Zareian F. Analyzing the Sufficiency of Alternative Scalar and Vector Intensity Measures of Ground Shaking Based on Information Theory. J Eng Mech 2012;138:307–16. doi:10.1061/(ASCE)EM.1943-7889.0000327.
[8] Mollaioli F, Lucchini A, Cheng Y, Monti G. Intensity measures for the seismic response prediction of base-isolated buildings. Bull Earthq Eng 2013;11:1841–66. doi:10.1007/s10518-013-9431-x.
[9] Bojórquez E, Iervolino I. Spectral shape proxies and nonlinear structural response. Soil Dyn Earthq Eng 2011;31:996–1008. doi:10.1016/j.soildyn.2011.03.006.
[10] Lucchini A, Mollaioli F, Monti G. Intensity measures for response prediction of a torsional building subjected to bi-directional earthquake ground motion. Bull Earthq Eng 2011;9:1499–518. doi:10.1007/s10518-011-9258-2.
[11] Padgett JE, Nielson BG, Desroches R. Selection of optimal intensity measures in probabilistic seismic demand models of highway bridge portfolios. Earthq Eng Struct Dyn 2008;37:711–

25. doi:10.1002/eqe.782.
[12] Kazantzi AK, Vamvatsikos D. Intensity measure selection for vulnerability studies of building classes. Earthq Eng Struct Dyn 2015;44:2677–94.
[13] Kohrangi M, Bazzurro P, Vamvatsikos D. Vector and scalar IMs in structural response estimation, Part I: Hazard Analysis. Earthq Spectra 2016;32:1507–24. doi:10.1193/053115EQS080M.
[14] Kohrangi M, Bazzurro P, Vamvatsikos D. Vector and scalar IMs in structural response estimation, Part II: Building demand assessment. Earthq Spectra 2016;32:1525–43. doi:10.1193/053115EQS081M.
[15] Kohrangi M, Vamvatsikos D, Bazzurro P. Implications of intensity measure selection for seismic loss assessment of 3-D buildings. Earthq Spectra 2016;32:2167–89. doi:10.1193/112215EQS177M.
[16] Seismosoft. SeismoStruct: A computer program for static and dynamic nonlinear analyzes of framed structures 2007.
[17] Smerzini C, Galasso C, Iervolino I, Paolucci R. Ground motion record selection based on broadband spectral compatibility. Earthq Spectra 2013;30:1427–48. doi:10.1193/052312EQS197M.
[18] Elnashai AS. Advanced inelastic static (pushover) analysis for earthquake applications. Struct Eng Mech 2001;12:51–69. doi:10.12989/sem.2001.12.1.051.
[19] Vamvatsikos D, Cornell CA. Incremental dynamic analysis. Earthq Eng Struct Dyn 2002;31:491–514. doi:10.1002/eqe.141.
[20] Jalayer F, Cornell CA. Alternative non-linear demand estimation methods for probability-based seismic assessments. Earthq Eng Struct Dyn 2002;38:951–72. doi:10.1002/eqe.876.
[21] Shome N, Cornell CA, Bazzurro P, Carballo JE. Earthquakes, records, and nonlinear responses. Earthq Spectra 1998;14:469–500. doi:10.1193/1.1586011.
[22] Mehanny SSF. A broad-range power-law form scalar-based seismic intensity measure. Eng Struct 2009;31:1354–68. doi:10.1016/j.engstruct.2009.02.003.
[23] Cordova PP, Deierlein GG, Mehanny SSF, Cornell CA. Development of a two-parameter seismic intensity measure and probabilistic design procedure. 2nd U.S.-Japan Work. PBEE Methodol. Reinf. Concr. Build. Struct., 2001.
[24] Regio Decreto 16/11/1939 n. 2229. Norme per la esecuzione delle opere in conglomerato cementizio semplice e armato. G.U. n. 92. 1940.
[25] Decreto Ministeriale del 30/05/1972. Norme tecniche alle quali devono uniformarsi le costruzioni in conglomerato cementizio, normale e precompresso ed a struttura metallica. (in Italian). Suppl Ordin Gazz Uff 1972.
[26] Decreto Ministeriale del 14/01/2008. Norme Tecniche per le Costruzioni. Rome: Gazzetta Ufficiale della Repubblica Italiana, 29.; 2008.
[27] De Luca F, Elefante L, Iervolino I, Verderame GM. Strutture esistenti e di nuova progettazione : comportamento sismico a confronto. Anidis 2009 XIII Convegno - L' Ing. Sismica Ital., Bologna: 2009.
[28] Mander J, Priestley M, Park R. Theoretical stress-strain model for confined concrete. J Struct Eng 1989;114:1804–26.
[29] Menegotto M, Pinto P. Method of analysis for cyclically loaded RC plane frames including changes in geometry and non-elastic behaviour of elements under combined normal force and bending. Proc. Symp. Resist. Ultim. Deform. Struct. anted by well Defin. loads., Lisbon, Portugal: 1973.
[30] Filippou F, Popov E, Bertero V. Effects of Bond Deterioration on Hysteretic Behavior of Reinforced Concrete Joints. Report EERC 83-19. 1983.
[31] Antoniou S, Pinho R. Development and verification of a displacement-based adaptive pushover procedure. J Earthq Eng 2004:643–661.
[32] EN 1998-1. Eurocode 8: Design of structures for earthquake resistance – Part 1: General rules, seismic actions and rules for buildings. The European Union Per Regulation 305/2011,

Directive 98/34/EC, Directive2004/18/EC; 2004.
[33] Jalayer F, Cornell CA. Alternative non-linear demand estimation methods for probability-based seismic assessments. Earthq Eng Struct Dyn 2009;38:951–72. doi:10.1002/eqe.876.
[34] Modica A, Stafford PJ. Vector fragility surfaces for reinforced concrete frames in Europe. Bull Earthq Eng 2014;12:1725–53. doi:10.1007/s10518-013-9571-z.
[35] Minas S, Chandler RE, Rossetto T. BEA: An efficient Bayesian emulation-based approach for probabilistic seismic response. Struct Saf 2018;74. doi:10.1016/j.strusafe.2018.04.002.
[36] Luco N, Cornell CA. Structure-specific scalar intensity measures for near-source and ordinary earthquake ground motions. Earthq Spectra 2007;23:357–92. doi:10.1193/1.2723158.
[37] Cover TM., Thomas JA. Elements of information theory. New York, USA: Wiley; 1991.
[38] Ebrahimian H, Jalayer F, Lucchini A, Mollaioli F, De Dominicis R. Case Studies on Relative Sufficiency of Alternative Intensity Measures of Ground Shaking. Second Eur. Conf. Earthq. Eng. Seismol. Istanbul 25-29, 2014, Istanbul: 2014, p. 12.
[39] Giovenale P, Cornell CA, Esteva L. Comparing the adequacy of alternative ground motion intensity measures for the estimation of structural responses. Earthq Eng Struct Dyn 2004;33:951–79. doi:10.1002/eqe.386.
[40] Minas S. Advancements in the seismic risk assessment of mid-rise reinforced concrete buildings. University College London, 2018.
[41] Kohrangi M, Kotha SR, Bazzurro P. Ground-motion models for average spectral acceleration in a period range: Direct and indirect methods. Bull Earthq Eng 2018;16:45–65. doi:10.1007/s10518-017-0216-5.
[42] Assatourians K, Atkinson GM. EqHaz: An Open-Source Probabilistic Seismic-Hazard Code Based on the Monte Carlo Simulation Approach. Seismol Res Lett 2013;84:516–24. doi:10.1785/0220120102.
[43] Meletti C, Galadini F, Valensise G, Stucchi M, Basili R, Barba S, et al. A seismic source zone model for the seismic hazard assessment of the Italian territory. Tectonophysics 2008;450:85-108.
[44] Barani S, Scafidi D, Eva C. Strain rates in northwestern Italy from spatially smoothed seismicity. J Geophys Res Solid Earth 2010;115. doi:10.1029/2009JB006637.
[45] Rossetto T, Elnashai AS. Derivation of vulnerability functions for European-type RC structures based on observational data. Eng Struct 2003;25:1241–63. doi:10.1016/S0141-0296(03)00060-9.
[46] Dolšek M, Fajfar P. The effect of masonry infills on the seismic response of a four-storey reinforced concrete frame — a deterministic assessment. Eng Struct 2008;30:1991–2001. doi:10.1016/j.engstruct.2008.01.001.
[47] Rossetto T, Ioannou I, Grant DN, Maqsood T. Guidelines for Empirical Vulnerability Assessment Report produced in the context of the Vulnerability Global Component project. Pavia, Italy: 2014.
[48] Bojórquez E, Iervolino I, Reyes-Salazar A, Ruiz SE. Comparing vector-valued intensity measures for fragility analysis of steel frames in the case of narrow-band ground motions. Eng Struct 2012;45:472–80. doi:10.1016/j.engstruct.2012.07.002.